energies

MDPI

Article

Automatic Optimization of Input Split and Bias Voltage in Digitally Controlled Dual-Input Doherty RF PAs

Mattia Mengozzi [1,*], Gian Piero Gibiino [1], Alberto Maria Angelotti [1], Alberto Santarelli [1], Corrado Florian [1,*] and Paolo Colantonio [2]

[1] Department of Electrical, Electronic, and Information Engineering "Guglielmo Marconi", University of Bologna, 40136 Bologna, Italy; gianpiero.gibiino@unibo.it (G.P.G.); alberto.angelotti@unibo.it (A.M.A.); alberto.santarelli@unibo.it (A.S.)

[2] Department of Electronic Engineering, University of Roma Tor Vergata, 00133 Rome, Italy; paolo.colantonio@uniroma2.it

* Correspondence: mattia.mengozzi3@unibo.it (M.M.); corrado.florian@unibo.it (C.F.)

Abstract: Digitally controlled Dual-Input Doherty Power Amplifiers (DIDPAs) are becoming increasingly popular due to the flexible input signal splitting between the main and auxiliary stages. Nevertheless, the presence of many degrees of freedom, e.g., input amplitude split and phase displacement as well as biasing for multiple stages, often involves inefficient trial-and-error procedures to reach a suitable PA performance. This article presents automated parameter setting based on coordinate descent or Bayesian optimizations, demonstrating an improvement in the performance in terms of RF output power and power-added efficiency (PAE) in the presence of broadband-modulated signals, yet maintaining suitable linear behavior for, e.g., communications applications.

Keywords: RF power amplifiers; Doherty amplifier; optimization; parameter search; digital input control; dual-input power amplifiers

Citation: Mengozzi, M.; Gibiino, G.P.; Angelotti, A.M.; Santarelli, A.; Florian, C.; Colantonio, P. Automatic Optimization of Input Split and Bias Voltage in Digitally Controlled Dual-Input Doherty RF PAs. *Energies* **2022**, *15*, 4892. https://doi.org/10.3390/en15134892

Academic Editor: Ahmed Abu-Siada

Received: 20 May 2022
Accepted: 30 June 2022
Published: 4 July 2022

1. Introduction

With the advent of the fifth generation of telecommunications (5G) and its deployment in Frequency Range 2 (FR2) as well as in new satellite-based telecom systems, Radio-Frequency (RF) systems increasingly require energy-efficient and broadband power amplification at microwave frequencies. RF power amplifiers (PAs) must feature high linearity to accommodate high-data-rate modulation standards while also displaying sufficient power-added efficiency (PAE). To meet these contrasting specifications, multi-stage PA transmitter topologies including features like dynamic load and supply modulation have been investigated in the recent past [1]. These PA architectures exploit multiple active devices and additional control signals to enhance PA performance across the wide dynamic range required by signals with high peak-to-average power ratio (PAPR).

Among the architectures based on load modulation, the Doherty PA (DPA) has found widespread application in the sub-6 GHz range [2], and it is nowadays being investigated at microwaves in the form of Microwave Monolithic Integrated Circuits (MMICs) [3]. In classical DPAs, the input signal is split by a 90-degree quadrature hybrid in order to feed an auxiliary (peaking) PA aimed at modifying the output impedance of a main PA at high power.

To establish proper DPA operation, the design flow should leverage accurate MMIC process design kits (PDKs). However, the synthesis of optimal loadlines for broadband signals at high operating frequencies is particularly problematic, as it is affected by the mutual dynamic load-pulling of the transistors employed in the two branches as well as the limited fractional bandwidth (BW) of the output combiner. While the availability of wideband active load-pull characterization techniques [4–6] should in principle allow the extraction of accurate models taking into account the global device behavior under

dynamic active injection, PDKs for MMICs are often validated in nominal conditions only, and may not be accurate enough for the successful design of MMIC DPAs at microwave frequencies.

Rather than establishing the behavior in hardware at the design stage, an alternative approach consists of leaving the additional parameters for load (or supply) modulation as digitally controlled external inputs. One example of such kind is the dual-input DPA (DIDPA) [7], where the input 90-degree quadrature hybrid is not implemented in hardware, and the two PA branches are left to be digitally controlled as independent inputs. The same applies to outphasing PAs [8], where the input signal separation network is often implemented digitally. While still permitting to implement digitally the exact nominal behavior of the corresponding hardware version, the availability of multiple control variables allows for higher flexibility in fine-tuning the overall PA performance. In effect, the additional degrees of freedom could in principle be used to concurrently optimize other Figures of Merit (FoMs), e.g., PAE. On the other hand, the identification of such an optimum might involve inefficient trial-and-error approaches or the non-trivial formulation of a high-dimensionality optimization problem. As a consequence, an active area of research concerns approaches based on numerical optimization or machine learning for optimal signal-input synthesis and operating point selection of digitally controlled PAs [9–13], and DIDPAs in particular [14,15].

In this work, we implement and compare optimization approaches for the optimal input splitting and biasing of a DIDPA under high-PAPR modulation. The DIDPA is designed in state-of-the-art 150 nm gallium nitride (GaN) on silicon carbide (SiC) MMIC technology with a center frequency of 24 GHz, targeting 5G FR2 applications. After defining the DIDPA optimization problem in Section 2, various optimization approaches are tested through a series of simulation-based experiments. A first approach (Section 3) investigates single-objective optimization with the *coordinate descent* algorithm, where the input variables are iteratively considered in pairs in order to maximize PAE. A second methodological solution employs a *Bayesian* approach to implement both a single-objective optimization (Section 4) as well as a global multi-objective optimization (MOO), where both the PAE and the RF output power are considered as joint target FoMs (Section 5). The latter leads to the extraction of a Pareto frontier of non-dominated solutions, namely corresponding to the value sets of input variables for which neither PAE nor RF output power can be improved without worsening the other. The performance of the PA optimal configurations obtained from the different optimization frameworks are discussed and evaluated for high-PAPR wideband-modulated signal excitation in Section 6.

2. DIDPA Optimization by Surrogate Modeling

2.1. DIDPA Design

The DIDPA here under analysis is designed exploiting the Win Semiconductors NP15-00 150 nm GaN process manufactured on 100 mm SiC wafers. This process is well suited for mm-wave high-power applications featuring $f_t = 34.5$ GHz. The breakdown voltage exceeds 100 V thanks to a source-coupled field plate. At 28 V operation, the maximum power density is 4 W/mm at 29 GHz. The DIDPA block diagram is shown in Figure 1, while its layout is shown in Figure 2. A two-stage amplification is used to target 25 dB of gain at 24 GHz. The devices of the driving stage are 2 × 75 µm HEMTs whereas, in the final stage, 6 × 75 µm HEMTs were used both for the main and the auxiliary PAs. The nominal drain voltage is V_D = 28 V for all the stages. In Figure 2, it is possible to visualize the asymmetry of the output combiner that provides the required 90-degree phase shift in the combination of the output signals. The chip dimensions are 3.8 mm × 4.2 mm.

The performance of the DIDPA enforcing the nominal input split and bias by applying the values from Table 1 (thus resulting in this case in a classical single-input DPA) is shown in Figure 3a,b, which respectively display the *S*-parameters and the continuous-wave (CW) large-signal characteristics. With a peak PAE of 40% and PAE of 30% at 6 dB of output

backoff, the performance of the presented PA is in line with similar K-band high-gain (two-stage) DPAs found in the literature, e.g., [16–18].

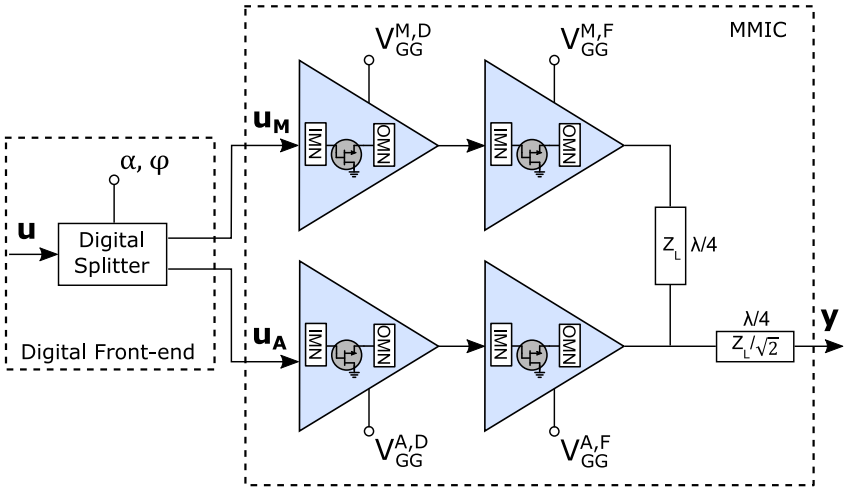

Figure 1. Block diagram of the DIDPA schematic with explicit labeling of the optimization variables (α, ϕ, $V_{GG}^{M,D}$, $V_{GG}^{M,F}$, $V_{GG}^{A,D}$, and $V_{GG}^{A,F}$), the main and auxiliary branch RF inputs (respectively, $\mathbf{u}_M$ and $\mathbf{u}_A$), and the RF output ($\mathbf{y}$). The block diagram highlights the two-stage DIDPA with the input and output matching networks (IMN and OMN) of each stage, and the quarter-wave output combiner.

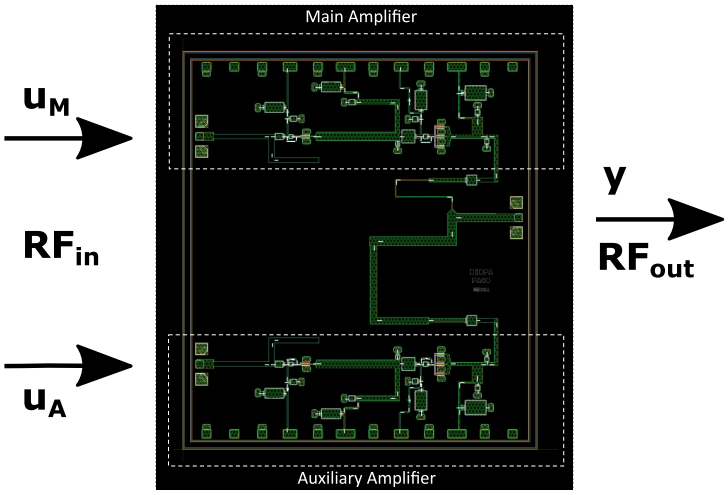

Figure 2. Layout of the simulated DIDPA MMIC with labeling of the main and auxiliary branch RF inputs (respectively, $\mathbf{u}_M$ and $\mathbf{u}_A$), and the RF output ($\mathbf{y}$).

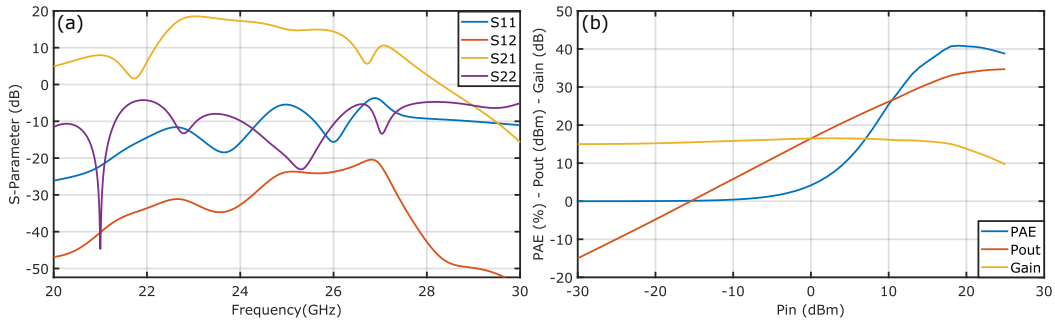

Figure 3. (**a**) *S*-parameters and (**b**) CW large-signal characteristic of the DIDPA when the nominal bias and input splitting are applied.

2.2. Definition of the Optimization Problem

The search for a set of best input variables resulting in optimal PA performance can be generally described as a MOO problem where the control inputs define a set **x** of variables, while the PA performance is quantified by multiple scalar FoMs (e.g., output power, PAE, gain) that constitute the multiple objectives of the problem and, as such, need to be maximized (or equivalently minimized). The definition of variables **x** clearly depends on the PA topology under study, e.g., the amplitude/phase split of the inputs in outphasing PAs or the injection ratio and input-referred phase displacement in load-modulated balanced amplifiers (LMBAs) [19].

For a DIDPA (see Figure 1), it is effective to consider as optimization variables the parameters of the input splitter, namely the amplitude ratio α and the phase displacement ϕ between the two split signals [14]. Moreover, the behavior of the DIDPA will critically depend on the biasing voltages of all stages, as they will determine the amplitude level at which the peaking amplifier will impact the main amplifier (and vice versa). Hence, it makes sense to consider all bias voltage values as additional optimization variables. For the case here under study, we consider the gate bias voltages for the driver and for the final PA of each of the DPA branches, namely for the main PA ($V_{GG}^{M,D}$ and $V_{GG}^{M,F}$, respectively) and for the auxiliary PA ($V_{GG}^{A,D}$ and $V_{GG}^{A,F}$, respectively). The six real variables here considered, along with their nominal values set in the design phase (prior to any optimization), are reported in Table 1.

Table 1. Nominal values of the parameters considered for DIDPA optimization.

α	ϕ (deg)	$V_{GG}^{M,D}$ (V)	$V_{GG}^{M,F}$ (V)	$V_{GG}^{A,D}$ (V)	$V_{GG}^{A,F}$ (V)
0.5	−90	−1.7	−1.7	−2.3	−2.1

The performance of the DIDPA can be evaluated through different FOMs, depending on the final application. The DIDPA here under analysis is targeted at wideband communication signals, so it should be assessed in terms of the compromise among PAE, RF output power, and linearity. More precisely, the FoMs to be optimized are here embodied by the following performance quantities:

$$\begin{aligned} \text{PAE}\ (\%) &= \frac{P_{out}^{RF} - P_{in}^{RF}}{P_{dc}}; \qquad P_{out}^{RF}\ (\text{W}) = \frac{1}{2NR_{out}} \sum_{n=0}^{N-1} |y_n|^2; \\ \text{NMSE}\ (\text{dB}) &= 10 \log_{10} \frac{\sum_{n=0}^{N-1} |y_n - G_{\text{lin}} u_n|^2}{\sum_{n=0}^{N-1} |G_{\text{lin}} u_n|^2}; \end{aligned} \tag{1}$$

where P_{dc} is the total power absorbed from the DC supply, P_{in}^{RF} is the sum of the RMS absorbed power at RF at the two inputs, $R_{out} = 50\ \Omega$ is the output resistance, u_n and y_n are, respectively, the complex envelope samples of the input (before digital split) and output signals, N is the number of time-domain signal samples, and G_{lin} is the desired linear gain for the device. It is important to note that the functional relationships underlying the FoMs in (1) are generally not known in an explicit mathematical formulation, since they depend on the complex nonlinear interactions taking place within the PA. Therefore, it is not typically feasible to solve the optimization problem in a closed form. On the other hand, the FoMs in (1) can be retrieved by direct evaluation for a set of given values of the input parameters by means of simulation- or measurement-based experiments.

An intuitive method for finding the maximum (or a minimum) of an objective function $g(\mathbf{x})$ describing a particular FoM without any hypothesis on the function itself (e.g., convexity) would consist of sweeping all variables (factorial sweep) across suitable value ranges. These can indeed be defined for the DIDPA variables in Table 1, namely $\alpha \in [0, 1]$, $\phi \in [-180, 180]$ (deg), while the remaining four bias voltage variables have limited ranges in order to respect the safe operating area of the transistors. However, the need for a suitable

resolution and the high dimensionality of the problem prevents the performing of a full factorial sweep. For example, a uniform factorial sweep would require r^6 FoM evaluations, with r being the number of evaluation points for each dimension, easily leading to several hundred-thousand FoM evaluations, which are clearly unbearable in either simulation- or measurement-based experiments.

While there exist suitable experiment designs for an efficient exploration of the variables' space [20], they would still require an excessively large number of evaluations for the application under study, still without any certainty of detecting the actual optima. Other optimization approaches available in the literature [21] are based on iterative algorithms, for example, including the calculation, at each iteration, of numerical gradients of the objectives and constraints. Gradient-based optimizers can be more efficient in selecting the actual direction for the optimum, and might be considered as an effective tool for DIDPA optimization [11]. However, gradient calculation requires a number of evaluations that is proportional to the number of the considered optimization variables (six in this case), and it is hence too unwieldy for a feasible implementation.

2.3. Surrogate Modeling and Considerations for Linearity with Modulated Signals

Beyond the considerations above, the evaluation of a PA FoM, i.e., of the objective function $g(\mathbf{x})$, either using measurements or envelope-transient simulations, can be particularly time consuming for orthogonal-frequency-division-multiplexing (OFDM) modulations involving a large number of carriers and long signal frames, as adopted in modern high-data-rate telecommunication standards. In order to make optimization feasible, in [13] it was proposed to exploit *surrogate* models (SUMOs) of the FoMs in (1), namely models that are fast in terms of extraction and evaluation, while also accurate enough to enhance convergence and steer the iterations towards the global optimum. In this work we follow the same approach by using multi-variable quasi-static AM/AM–AM/PM characteristics as the basis for DIDPA surrogate modeling. Such a surrogate description can jointly handle the six considered variables, and can be straightforwardly and efficiently evaluated by standard CW single-tone experiments.

To calculate FoM prediction in the presence of modulated signals from the quasi-static SUMO, the DIDPA quasi-static CW characteristics should be weighted by the probability density function (PDF) of the stationary stochastic process corresponding to the excitation signal class of interest [22,23]. In the case under consideration, the class of OFDM-modulated signals asymptotically corresponds to a Gaussian complex envelope [24], thus to a signal amplitude matching a Rayleigh distribution. Therefore, the RF output power (P_{out}^{RF}) and the PAE can be written as follows:

$$P_{out}^{RF} = \int_0^{+\infty} P_{out}^{pdf}(p)dp; \quad \text{PAE} = \frac{\int_0^{+\infty} P_{out}^{pdf}(p)dp - \int_0^{+\infty} \widehat{P}_{in}(p)P_{out}^{pdf}(p)dp}{\int_0^{+\infty} \widehat{P}_{dc}(p)P_{out}^{pdf}(p)dp}; \tag{2}$$

where $P_{out}^{pdf}(p)$ is the probability density function of the desired output-modulated signal, $\widehat{P}_{in}(p)$ is the static relationship between the output p and the input $\widehat{P}_{in}$ power of the DIDPA, and $\widehat{P}_{dc}(p)$ is the static relationship between the output p and the absorbed power at DC. Calculating FoMs with Equation (2) is conceptually equivalent to exciting the quasi-static SUMO model with a modulated signal. While such a quasi-static SUMO representation might be suboptimal for wideband signals, it will be shown that for the case under examination it provides sufficient ability to sort out the main interdependencies among the input variables and it proves effective for the optimization. The actual DIDPA broadband behavior can always be checked with a final experimental assessment under a wideband signal excitation. In this context, the aim is to see the FoMs calculated with the PDF-based SUMO in (2) converge to the values calculated under a wideband signal excitation in (1).

The choice of the optimization algorithm is critical as it determines the number of iterations and FoM evaluations needed to reach a solution, and the complexity involved

becomes particularly high when considering multiple objectives. In this context, the RF output power and the PAE as defined in (2) will be used as the key FoMs to evaluate PA performance. Regarding linearity, let us exploit the adopted SUMO representation considering that the typical AM/AM–AM/PM characteristics of a well-designed PA are monotonic and thus biunivocal, and hence analytically invertible [13,25]. In other words, given a theoretically *infinite* complexity for the predistorter, the AM/AM–AM/PM characteristics can be exactly linearized, and hence always respect any required NMSE constraint.

Although the hypothesis of exact linearization (i.e., resulting in infinite DPD complexity) is clearly unrealistic, non-parametric DPD methods like Iterative Learning Control (ILC) [26] allow to find the ideal predistorted waveform (up to the numeric precision) for a given PA regime. While the actual parametric predistorter implementation (with a finite set of DPD coefficients) will clearly entail higher NMSEs, DPD complexity nowadays available in hardware for communications applications can typically accommodate sufficient linearization performance. Therefore, the NMSE constraint will not be explicitly accounted for in the optimization methods described in Sections 3 and 4 to be applied to the quasi-static AM/AM–AM/PM SUMO. The optima found with these methods will then be tested in Section 6 under wideband modulated excitation in order to validate this assumption.

3. Coordinate Descent Optimization

The *coordinate descent* (CD) algorithm finds the local optimum of the target objective function $g(\mathbf{x})$ by successively solving a maximization (or minimization) problem along a limited set of coordinate directions. In practice, a subset of the six control variables $\mathbf{x}$ of the DIDPA is selected, and the optimum is searched across this subset while blocking the other variables to fixed values. The procedure is then repeated by cycling through the other subsets of variables, optimizing one subset at a time. Provided that the multivariable dependency of the objective function $g(\mathbf{x})$ (i.e., the target FoM) is smooth, as expected in the considered DIDPA configuration, the method allows for a drastic reduction of FoM evaluations, as each of the iterations deals with a problem of lower dimensionality.

In particular, the six variables in Table 1 are divided into three subsets of two variables each, namely the splitting variables (α,ϕ), the biasing of the main PA ($V_{GG}^{M,D}$,$V_{GG}^{M,F}$), and the biasing of the auxiliary PA ($V_{GG}^{A,D}$,$V_{GG}^{A,F}$). This configuration makes it feasible to find the optimum across a 2D space by means of 2D factorial sweep with sufficient resolution (Table 2). Figure 4 reports an example of the 2D sweeps for each iteration, showing that the dependency of PAE on the variables is sufficiently regular in the application domain, allowing to easily select the maximum point at each cycle.

Table 2. Resolutions of the variables employed in the 2D factorial sweeps.

α	ϕ (deg)	$V_{GG}^{M,D}$ (V)	$V_{GG}^{M,F}$ (V)	$V_{GG}^{A,D}$ (V)	$V_{GG}^{A,F}$ (V)
0.01	1	0.1	0.1	0.1	0.1

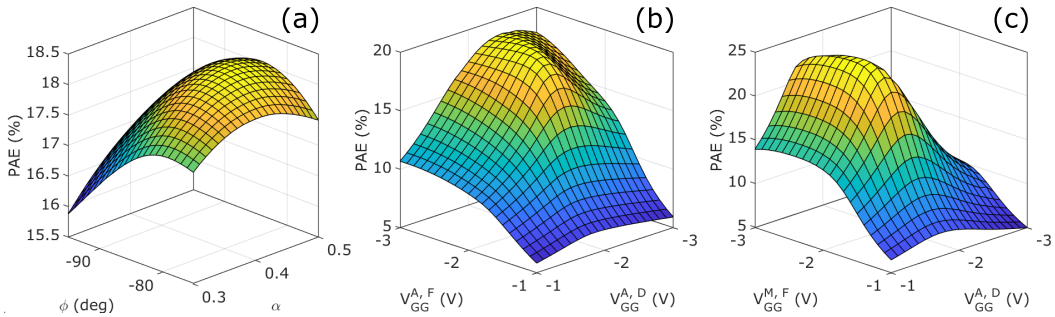

Figure 4. Example of 2D sweeps cyclically realized by the coordinate descent optimization of PAE for the DIDPA under study versus (**a**) input splitter parameters (α, ϕ), (**b**) auxiliary amplifier bias voltages ($V_{GG}^{A,D}$, $V_{GG}^{A,F}$), and (**c**) main amplifier bias voltages ($V_{GG}^{M,D}$, $V_{GG}^{M,F}$).

Figure 5 displays the flow chart for the CD algorithm applied to the quasi-static AM/AM–AM/PM SUMO and aimed at the maximization of the PAE metric as defined in (2). In the depicted flow chart, the sequence and selection of variables for optimization is fixed in the order $(\alpha,\phi) \rightarrow (V_{GG}^{A,D},V_{GG}^{A,F}) \rightarrow (V_{GG}^{M,D},V_{GG}^{M,F})$. However, any other different permutation could be adopted (see below).

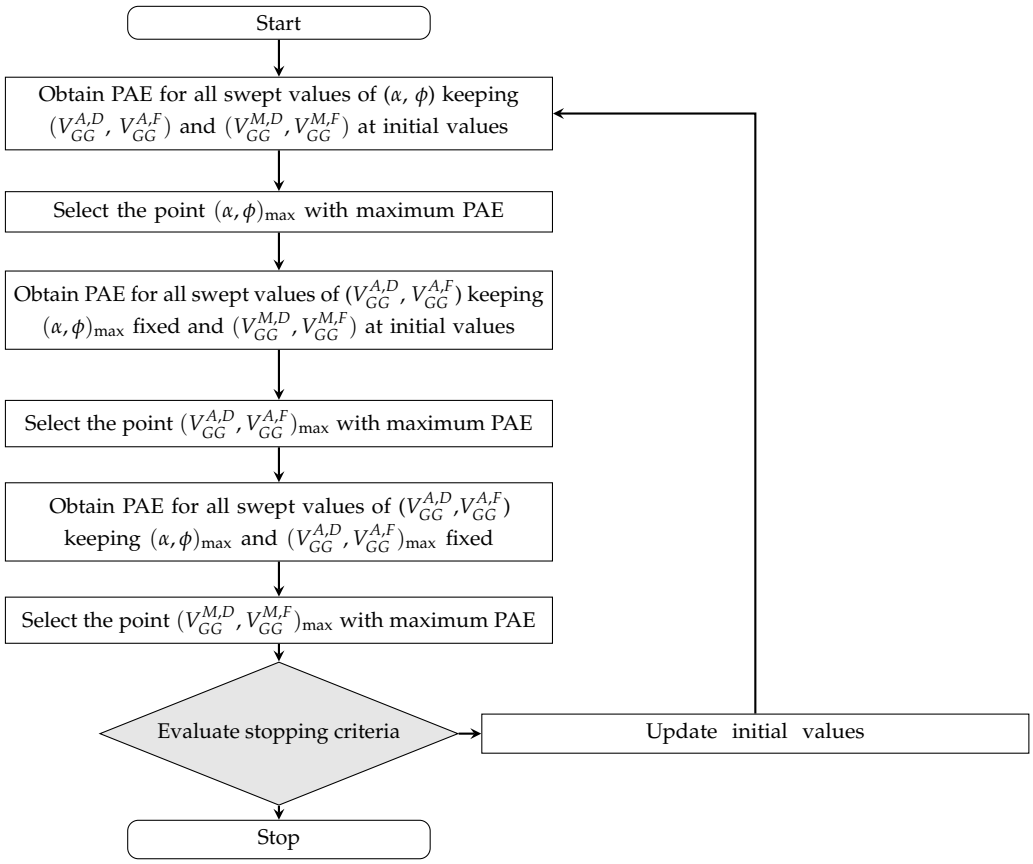

Figure 5. Flow chart for the coordinate descent optimization algorithm for the case of descent order $(\alpha,\phi) \rightarrow (V_{GG}^{A,D},V_{GG}^{A,F}) \rightarrow (V_{GG}^{M,D},V_{GG}^{M,F})$.

Firstly, the splitter parameters (α, ϕ) are swept while keeping the biasing parameters fixed at nominal values (Table 1) so as to identify a point $(\alpha,\phi)_{max}$ corresponding to the maximum PAE across the 2D domain defined by the splitter. Then, the same procedure is applied to the bias voltages of the auxiliary amplifier ($V_{GG}^{A,D}$, $V_{GG}^{A,F}$), while the splitter parameters are fixed at $(\alpha,\phi)_{max}$. Once the point $(V_{GG}^{A,D}, V_{GG}^{A,F})_{max}$ corresponding to the maximum PAE among the swept values has been identified, the same procedure is eventually repeated for the main amplifier bias voltages ($V_{GG}^{M,D}$, $V_{GG}^{M,F}$).

The adopted descent order may clearly have an impact on the optimum found by the algorithm. Thus, all the permutations have been tested, and the results after one iteration of the flow chart in Figure 5 are reported in Table 3. The relatively small differences suggest that all orders identify a similar optimum, making CD a reliable solution for this optimization problem.

In addition, the same flow chart can also be iterated. Thus, as further tested, we considered the order achieving the best PAE in the first iteration, namely $(V_{GG}^{M,D},V_{GG}^{M,F}) \rightarrow (V_{GG}^{A,D},V_{GG}^{A,F}) \rightarrow (\alpha,\phi)$, and left it iterating until no incremental improvement could be seen between two successive iterations. In Table 4, we compare the results between the case with only one iteration and the iterative case (six iterations in total, with a proportional number of PAE evaluations involved), reporting only a small increment in PAE. It is worth highlighting that the retrieval of the PAE value for a given set of input variables corresponds

to the evaluation of the quasi-static PAE expression in (2), which is very quick in a classical PC simulation environment (in the order of a few seconds), thus making it feasible to realize the high number of PAE evaluations as the ones reported in Table 4.

Table 3. Comparison among optimum DIDPA performance obtained by applying the coordinate descent algorithm to the quasi-static SUMO for PAE maximization. All optimized performances involve the ILC-based analytical linearization of the quasi-satic SUMO during the optimization.

Coordinate Descent Order	P_{out}^{RF} (dBm)	PAE (%)
$(\alpha,\phi) \rightarrow (V_{GG}^{A,D},V_{GG}^{A,F}) \rightarrow (V_{GG}^{M,D},V_{GG}^{M,F})$	24.0	24.5
$(\alpha,\phi) \rightarrow (V_{GG}^{M,D},V_{GG}^{M,F}) \rightarrow (V_{GG}^{A,D},V_{GG}^{A,F})$	23.9	24.1
$(V_{GG}^{M,D},V_{GG}^{M,F}) \rightarrow (\alpha,\phi) \rightarrow (V_{GG}^{A,D},V_{GG}^{A,F})$	24.2	24.3
$(V_{GG}^{A,D},V_{GG}^{A,F}) \rightarrow (V_{GG}^{M,D},V_{GG}^{M,F}) \rightarrow (\alpha,\phi)$	24.0	25.2
$(V_{GG}^{M,D},V_{GG}^{M,F}) \rightarrow (\alpha,\phi) \rightarrow (V_{GG}^{A,D},V_{GG}^{A,F})$	23.8	25.0
$(V_{GG}^{M,D},V_{GG}^{M,F}) \rightarrow (V_{GG}^{A,D},V_{GG}^{A,F}) \rightarrow (\alpha,\phi)$	23.9	25.3

Table 4. Comparison among nominal and optimum DIDPA performance obtained by applying the various single-objective optimization algorithms to the quasi-static SUMO for PAE maximization. All optimized performances involve the ILC-based analytical linearization of the quasi-static SUMO during the optimization.

Algorithm	P_{out}^{RF} (dBm)	PAE (%)	Nr of PAE Evaluations
Nominal (no optim)	24.2	18.2	–
Coordinate descent $(V_{GG}^{M,D},V_{GG}^{M,F}) \rightarrow (V_{GG}^{A,D},V_{GG}^{A,F}) \rightarrow (\alpha,\phi)$	23.9	25.3	1730
Coordinate descent (iterated) $(V_{GG}^{M,D},V_{GG}^{M,F}) \rightarrow (V_{GG}^{A,D},V_{GG}^{A,F}) \rightarrow (\alpha,\phi)$	23.4	26.2	10,380
Bayesian	23.6	26.1	100

4. Bayesian Optimization

The Bayesian optimization (BO) algorithm aims at minimizing an unknown scalar objective function that is expensive to evaluate (e.g., the evaluation is expensive in terms of time or resources, or the number of times the objective function can be evaluated is otherwise limited). The approach itself may be placed in the general class of surrogate methods as it exploits a SUMO to find the expected minimum at every iteration. The SUMO is extracted from a dataset $\mathcal{D}$ composed by the previous evaluations exploiting a regression algorithm and updated with new samples at every iteration.

The peculiar aspect of BO consists of using a stochastic model $\tilde{g}(\mathbf{x})$ as SUMO [27]. In this context, $\tilde{g}(\mathbf{x})$ does not directly provide a deterministic prediction of the value of $g(\mathbf{x})$ in the evaluated point, but it represent a stochastic process. Therefore, $\tilde{g}(\mathbf{x})$ assigns to every possible $\mathbf{x}$ a random variable whose distribution represents the probability of $g(\mathbf{x})$ assuming a particular value. The typical SUMO for Bayesian optimization is the Gaussian Regression Model (RGM) which, in this work, is extracted on top of the baseline quasi-static SUMO made of AM/AM–AM/PM characteristics of the DIDPA, as discussed in Section 2. The RGM is based on the class of Gaussian processes, which are fully characterized by their covariance function [28].

Two key elements must be defined for implementing BO:

1. A parametric model for the Gaussian process covariance function. The parameters of this model represent the hyperparameters of the SUMO, which are updated at every iteration using the samples of $g(\mathbf{x})$. The basis functions that are typically used in these

applications are the radial basis functions or squared exponential functions. In this work, the covariance model is based on the *Matern functions* (the *Matern functions* are the default basis functions adopted by the MATLAB *bayesopt* routine used in this work) [28].

2. The acquisition function (AF) is used to estimate the location of the minimum/maximum of interest. Since the RGM does not provide a deterministic value for the SUMO estimation, it is necessary to choose a function that selects the predicted value among all possible ones. Therefore, the AF takes the stochastic process as the input, and it provides a deterministic function, whose minimum/maximum is the point that will be evaluated by the objective function. One possible strategy is to choose the AF that calculates the expected improvement or the probability of improvement in the evaluated point [29]. The AF used in this work is called *lower confidence bound*:

$$a(\mathbf{x}) = \mu(\mathbf{x}) - w\sigma(\mathbf{x}), \tag{3}$$

where $\mu(\mathbf{x})$ and $\sigma(\mathbf{x})$ are, respectively, the mean and the variance of the Gaussian process in the evaluated point $\mathbf{x}$, while w is a scalar parameter used to select the tradeoff between exploring unknown points or searching new optima close to the previously expected ones.

Figure 6 outlines the basic steps of the adopted algorithm. At every iteration n, the method extracts the Gaussian process used as SUMO from the dataset $\mathcal{D}_n$, which is the collection of all the evaluations of the objective function $g(\mathbf{x})$ at that iteration. Then, it selects the point $\mathbf{x}_n$ that should be evaluated next by minimizing the AF. At the end of every iteration, the method evaluates the exit conditions, which in this case are set as a maximum number of iterations without an improvement of the objective function.

The result of applying this algorithm to maximize the PAE of (2) from the baseline quasi-static SUMO (AM/AM–AM/PM characteristics) of the DIDPA is shown in Table 4. The BO results in a similar optimal point as the iterative version of CD, but it requires much less evaluations of the objective function.

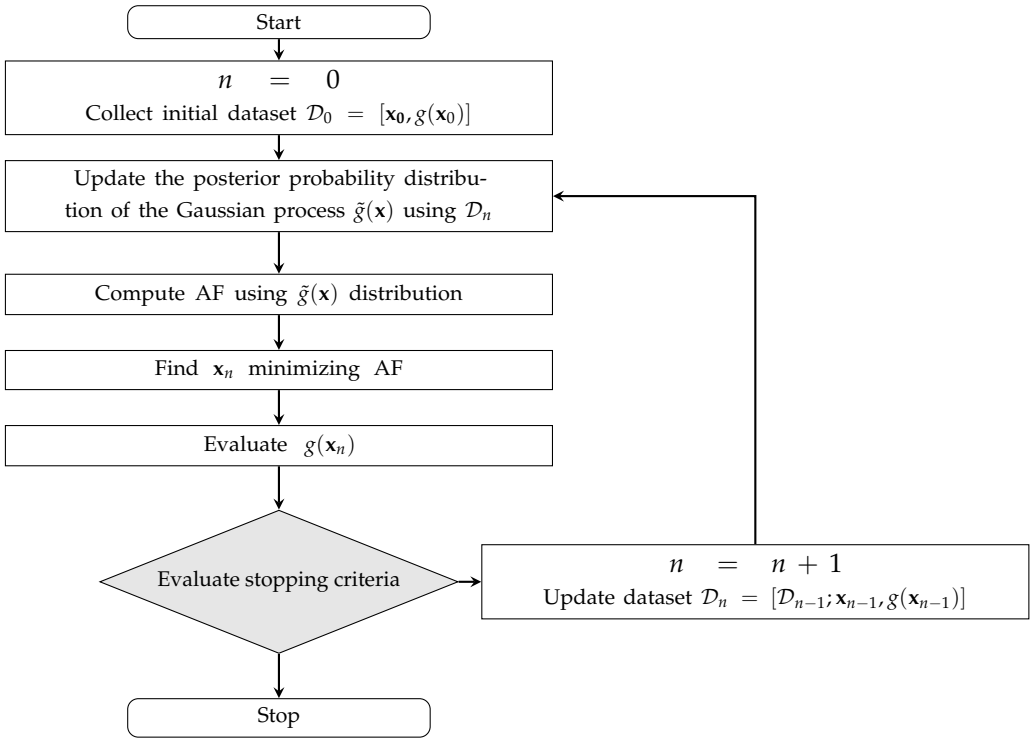

Figure 6. Flow chart for single-objective Bayesian optimization.

5. Multi-Objective Bayesian Optimization

It is of clear interest for PA application to optimize not only the PAE (single-objective optimization), but the compromise between PAE and RF output power. Table 4 highlights a trade-off between PAE and P_{out}^{RF}, since the points found optimizing the PAE show a lower level of P_{out}^{RF}. In order to preliminarily visualize such a trade-off for the DIDPA under study, Figure 7 reports an extensive sampling of the variables' space from a high number of evaluations of the quasi-static SUMO, reporting the ILC-based linearized performance on the 2D plane of the objectives. The solution points highlighted with red circles identify the non-dominated points (Pareto frontier) representing best PAE–RF output power trade-offs.

Rather than performing an unfeasibly high amount of function evaluations, an efficient way to identify the Pareto frontier consists of combining the FoMs to be optimized in a single scalar objective function $g(\mathbf{x})$ and thus adopt a single-objective optimization algorithm such as in the previously described CD or BO cases. In particular, the BO was chosen for this test given that it compared favorably with respect to CD. A polynomial combination among two different FoMs is considered:

$$g(\mathbf{x}) = \lambda f_1(\mathbf{x})^k + (1-\lambda) f_2(\mathbf{x})^k; \qquad \text{with } \lambda \in [0,1]; \tag{4}$$

where k is the polynomial order, λ is the combination parameter, while $f_1(\mathbf{x})$ and $f_2(\mathbf{x})$ are normalized scalar FoMs.

Considering the DIDPA, the scalar FoMs to be used in the problem in (4) are obtained from the PAE and P_{out}^{RF} in (2) by means of the following normalization:

$$f_1(\mathbf{x}) = 1 - \frac{PAE(\mathbf{x}) - PAE_{min}}{PAE_{max} - PAE_{min}}; \qquad f_2(\mathbf{x}) = 1 - \frac{P_{out}^{RF}(\mathbf{x}) - P_{\text{out, min}}^{RF}}{P_{\text{out, max}}^{RF} - P_{out,min}^{RF}}; \tag{5}$$

where PAE_{max} is the result of single-objective PAE maximization, while PAE_{min} is the PAE value in the point that maximizes P_{out}^{RF}. $P_{\text{out, max}}^{RF}$ is the result of the single objective P_{out}^{RF} maximization, while $P_{\text{out, min}}^{RF}$ is the P_{out}^{RF} value in the point that maximizes PAE. The set of optimal points have then be obtained by sweeping λ from 0 to 1 with the aim to identify the non-dominated points of the Pareto frontier. Each of the points is obtained through one iterative single-objective optimization of the quasi-static SUMO of the DIDPA as depicted in Figure 6, where $\lambda = 0$ corresponds to P_{out}^{RF} maximization (f_2 minimization), while $\lambda = 1$ corresponds to PAE maximization (f_1 minimization).

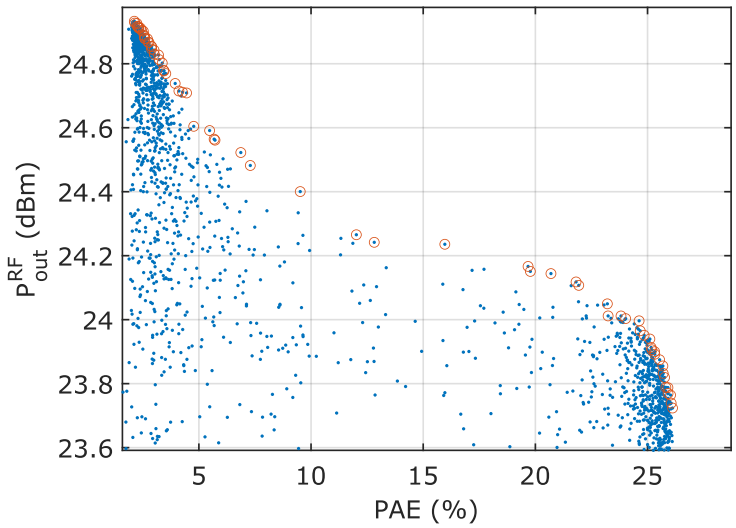

Figure 7. Sampling of the six-dimensional variable space showing many possible trade-off points between RMS RF output power and PAE, highlighting the profile of non-dominated points (Pareto frontier).

Clearly, the way the FoMs are summed influences the results [30]. Figure 8 reports the optimal points against the normalized FoMs, showing the effects of changing the order k of the polynomial combination within the optimization. In particular, Figure 8a, reports the use of a linear combination ($k = 1$), showing that, in this case, it is not possible to identify optimal points laying in the non-convex region of the normalized Pareto front. Indeed, the algorithm provides those optima best favouring either f_1 or f_2, but not their concurrent combination, given that the points in the non-convex region do not actually represent a minimum for the combined objective function. Conversely, Figure 8b shows the estimated Pareto frontier with $k = 3$, allowing to identify the non-dominated trade-off points in the non-convex region.

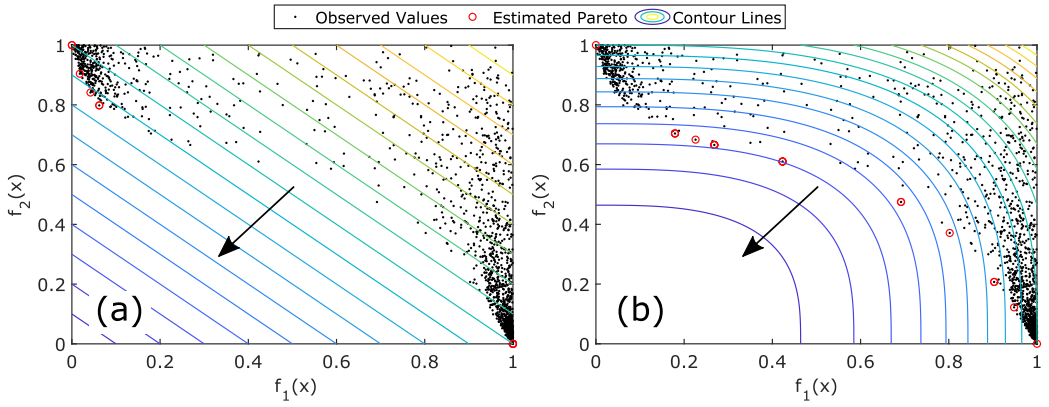

Figure 8. Estimated optimal points (red circles) in a non-convex Pareto frontier with different FoM combinations with contour lines of the combined objective function for $\lambda = 0.5$. (**a**) Linear combination ($k = 1$), (**b**) non-linear combination ($k = 3$). The arrows indicate the combined minimization of the two scaled FoMs.

Figure 9 displays the same results as Figure 8, yet de-normalized to the actual P_{out}^{RF} and PAE values. Figure 9a shows the trade-off points obtained by performing the MOO based on a linear combination of the objectives ($k = 1$), which is not able to converge to the optimal trade-off points in the non-convex region of the Pareto frontier previously reported in Figure 7. The case using the non-linear combination ($k = 3$) is instead able to identify the non-convex region of the Pareto front. The latter thus demonstrates the possibility of extracting the Pareto frontier in an efficient way by BO.

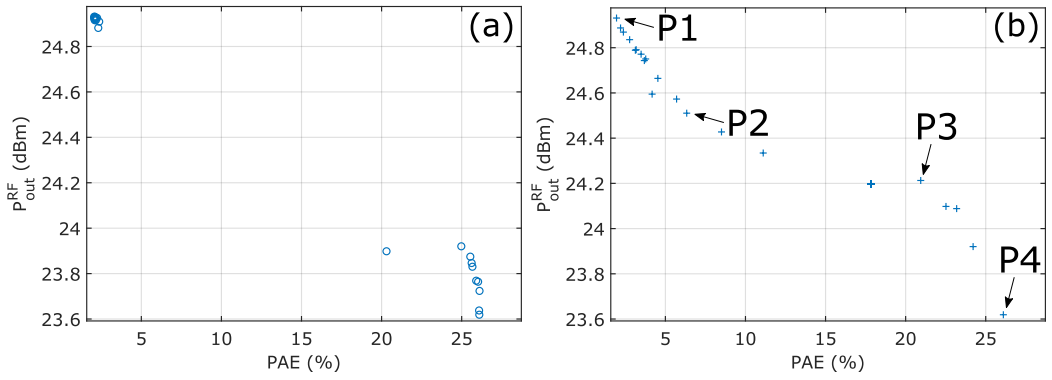

Figure 9. Estimated Pareto frontier between RMS RF output power and PAE obtained with a (**a**) linear combination ($k = 1$) and (**b**) non-linear combination ($k = 3$), while sweeping the combination factor λ.

In Figure 9b, P1 and P4 are the values for maximum P_{out}^{RF} and PAE, identified by optimizing the combined objective function with $\lambda = 0$ and $\lambda = 1$, respectively. P2 and P3 represent two possible compromises between P_{out}^{RF} and PAE, and they are, respectively, obtained with $\lambda = 0.16$ and $\lambda = 0.84$. The results related to these points are summa-

rized in Table 5, where they are compared with the values previously obtained with the CD algorithm.

Table 5. Comparison of PA performances obtained by means of PDF-based SUMO simulation at the optimal points.

Algorithm	λ	P_{out}^{RF} (dBm)	PAE (%)	Nr of Function Evaluations
Nominal (no optim)	–	24.2	18.2	–
Coordinate descent (iterated)	–	23.4	26.2	10,380
Bayesian P1	0	24.9	2.0	100
Bayesian P2	0.16	24.5	6.3	100
Bayesian P3	0.84	24.2	20.0	100
Bayesian P4	1	23.6	26.1	100

6. DIDPA Performance under Wideband Modulation

The optimal points based on the quasi-static SUMO (Table 4) must be validated under actual wideband-modulated signals, thus accounting for the DIDPA dynamic effects. This validation is here performed by circuit envelope (CE) simulations with a random phase multitone as input test signal, whose statistics can be setup to faithfully reproduce modern 5G signals [31]. The adopted signal BW and tone spacing are 100 MHz and 10 kHz, respectively, resulting in a 10k-tone signal with PAPR = 10.4 dB. Coherently with the considerations in Section 2, the non-parametric ILC algorithm was applied in order to linearize the DIDPA.

The test results of the single-objective optimization for PAE maximization by CD (Section 3) and BO (Section 4) are reported in Table 6. First of all, it should be noted that the nominal DIDPA configuration without optimization displays a reduction of more than 2% in terms of PAE and 0.4 dB of RMS RF output power with respect to the PDF-based evaluation of the quasi-static SUMO in Table 4. This difference is expected, due to the dynamics accounted for by the multitone CE simulation.

Also under actual high-PAPR-modulated excitation, the optimized performance obtained provides a substantial improvement with respect to the nominal conditions (up to $\sim$ 8% of absolute PAE increase), although slightly worse than the one predicted by the PDF-based quasi-static SUMO in Table 4. The results are similar between CD and BO, although BO takes much fewer evaluations. The hypothesis of sufficient linearization is demonstrated by the fact that both the adjacent-channel power ratio (ACPR) and NMSE are low enough with respect to the typical specifications of telecom standards.

Figure 10 shows the spectra before and after the ILC-based linearization of the DIDPA with nominal parameters, and for the optimal points identified by the CD and the BO, corresponding to the performance FoMs reported in Table 6. The same data are depicted in Figure 11 in terms of dynamic gain and AM/PM characteristics.

Those optimal trade-off points identified by the MOO described in Section 5 were also validated under the same modulated excitation. In particular, optimal points P1–P4 are reported in Table 6, demonstrating a very good alignment with Table 5 and the effectiveness of the SUMO-based optimization, despite the slightly reduced overall performance. Also in these cases, the linearity performance is satisfactory with respect to the specifications by telecom standards. Table 7 reports the values of the optimization variables corresponding to the FoMs shown in Table 6. In the case of single-objective PAE maximization (i.e., in the CD method and Bayesian P4 point), Table 7 highlights that BO and iterated CD deliver almost the same operating point, although many fewer function evaluations are needed for

BO (see Table 5). This relatively fast convergence property allows the efficient exploration of the Pareto frontier by means of a series of single-objective optimization. In order to show the linearization performance achieved in the optimal point P3 by BO, Figures 12 and 13, respectively, show the spectra, gain and AM/PM characteristics of the DIDPA before (blue curves) and after (red curves) the ILC-based linearization.

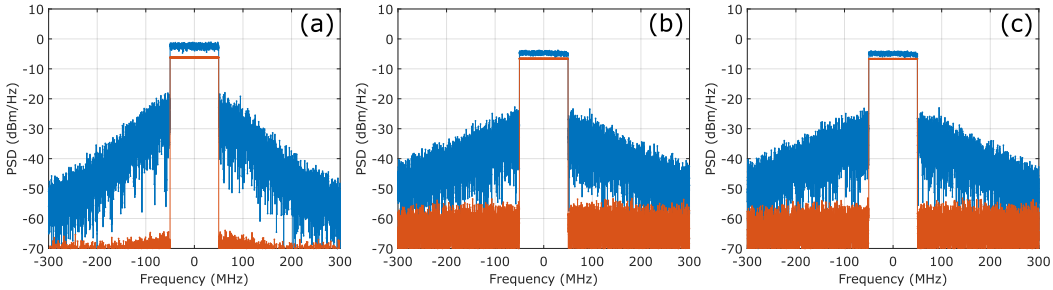

Figure 10. Spectra of the output RF signal before (blue lines) and after linearization (red lines) with PA parameters at (**a**) nominal values, (**b**) after coordinate descent (iterated) optimization, and (**c**) after Bayesian optimization (P4).

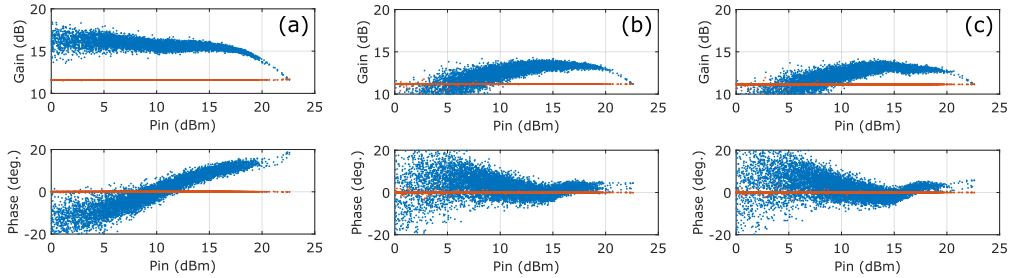

Figure 11. PA gain and AM/PM characteristics before (blue lines) and after linearization (red lines) with PA parameters at (**a**) nominal values, (**b**) after coordinate descent (iterated) optimization, and (**c**) after Bayesian optimization (P4).

Table 6. Comparison of PA performances obtained by means of envelope simulation with modulated signals at the optimal points found running the coordinate descent or Bayesian optimizations on the PDF-based SUMO.

Algorithm	λ	P_{out}^{RF} (dBm)	PAE (%)	ACPR (dB)	NMSE (dB)
Nominal	–	23.8	16.7	−65.6	−59.0
Coordinate descent (best permutation)	–	23.5	24.0	−56.7	−50.1
Coordinate descent (iterated)	–	23.4	24.6	−54.5	−47.8
Bayesian P1	0	25.0	2.0	−52.8	−46.1
Bayesian P2	0.16	24.1	6.0	−56.2	−47.8
Bayesian P3	0.84	23.7	20.0	−60.2	−53.6
Bayesian P4	1	23.4	24.6	−52.2	−45.7

Table 7. Nominal values of the parameters considered for DIDPA optimization.

Algorithm	α	ϕ (deg)	$V_{GG}^{M,D}$ (V)	$V_{GG}^{M,F}$ (V)	$V_{GG}^{A,D}$ (V)	$V_{GG}^{A,F}$ (V)
Nominal	0.5	−90	−1.7	−1.7	−2.3	−2.1
Coordinate descent (best permutation)	0.5	−80	−1.8	−2.3	−2.5	−2.7
Coordinate descent (iterated)	0.6	−75	−1.9	−2.5	−2.4	−2.9
Bayesian P1	0.49	−87	−0.6	−0.3	−0.5	−0.1
Bayesian P2	0.21	−69	−1.1	−2.0	−1.0	−1.4
Bayesian P3	0.43	−81	−1.7	−2.2	−2.2	−2.2
Bayesian P4	0.61	−75	−1.9	−2.6	−2.4	−2.9

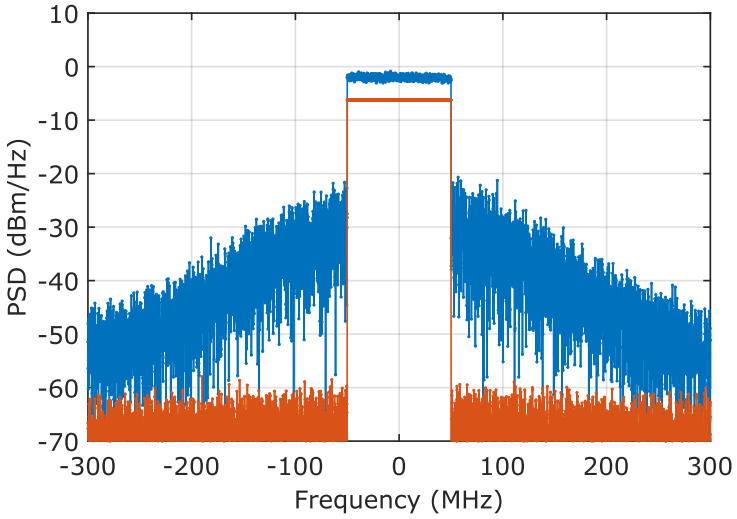

Figure 12. RF output spectrum before (blue lines) and after linearization (red lines) at optimal point P3.

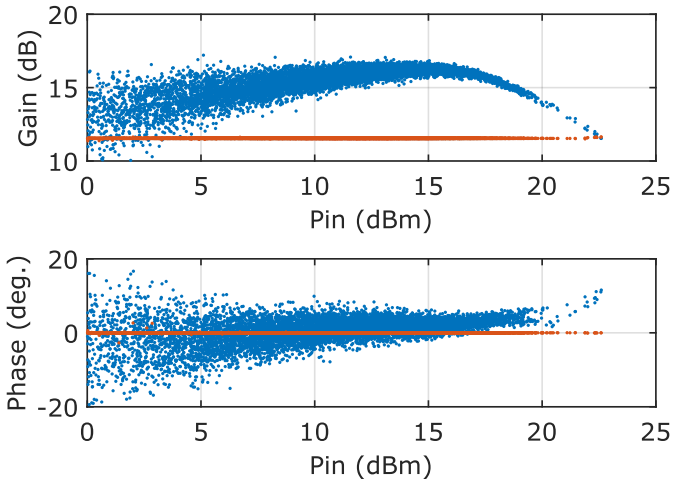

Figure 13. PA gain and AM/PM characteristics before (blue lines) and after linearization (red lines) at optimal point P3.

Author Contributions: Conceptualization, M.M., G.P.G., A.M.A. and C.F.; methodology, G.P.G. and A.M.A.; software, M.M.; validation, M.M.; formal analysis, M.M., G.P.G. and A.M.A.; investigation, M.M., G.P.G. and A.M.A.; resources, C.F. and P.C.; data curation, M.M.; writing—original draft preparation M.M., A.M.A. and G.P.G.; writing—review and editing, G.P.G., A.M.A., C.F. and A.S.; supervision, G.P.G., C.F., A.S. and P.C. All authors have read and agreed to the published version of the manuscript.

Funding: This research received no external funding.

Institutional Review Board Statement: Not applicable.

Informed Consent Statement: Not applicable.

Data Availability Statement: The data presented in this study are available on request from the corresponding author.

Acknowledgments: The authors would like to thank the Microwave Engineering Center for Space Applications (MECSA) and WIN Semiconductors for providing the access to the NP15-00 150 nm GaN on SiC process and the model used to design the DIDPA.

Conflicts of Interest: The authors declare no conflict of interest.

References

1. Lavrador, P.M.; Cunha, T.R.; Cabral, P.M.; Pedro, J. The linearity-efficiency compromise. *IEEE Microw. Mag.* **2010**, *11*, 44–58. [CrossRef]
2. Chen, W.; Lv, G.; Liu, X.; Wang, D.; Ghannouchi, F.M. Doherty PAs for 5G massive MIMO: Energy-efficient integrated DPA MMICs for sub-6-GHz and mm-wave 5G massive MIMO systems. *IEEE Microw. Mag.* **2020**, *21*, 78–93. [CrossRef]
3. Piacibello, A.; Giofrè, R.; Quaglia, R.; Figueiredo, R.; Carvalho, N.; Colantonio, P.; Valenta, V.; Camarchia, V. A 5-W GaN Doherty Amplifier for Ka-Band Satellite Downlink With 4-GHz Bandwidth and 17-dB NPR. *IEEE Microw. Wirel. Compon. Lett.* **2022**. . [CrossRef]
4. Marchetti, M.; Pelk, M.J.; Buisman, K.; Neo, W.E.; Spirito, M.; de Vreede, L.C. Active harmonic load–pull with realistic wideband communications signals. *IEEE Trans. Microw. Theory Tech.* **2008**, *56*, 2979–2988. [CrossRef]
5. Hallberg, W.; Nopchinda, D.; Fager, C.; Buisman, K. Emulation of Doherty amplifiers using single-amplifier load–pull measurements. *IEEE Microw. Wirel. Compon. Lett.* **2019**, *30*, 47–49. [CrossRef]
6. Angelotti, A.M.; Gibiino, G.P.; Nielsen, T.S.; Schreurs, D.; Santarelli, A. Wideband active load–pull by device output match compensation using a vector network analyzer. *IEEE Trans. Microw. Theory Tech.* **2020**, *69*, 874–886. [CrossRef]
7. Darraji, R.; Ghannouchi, F.M.; Hammi, O. A dual-input digitally driven Doherty amplifier architecture for performance enhancement of Doherty transmitters. *IEEE Trans. Microw. Theory Tech.* **2011**, *59*, 1284–1293. [CrossRef]
8. Barton, T. Not just a phase: Outphasing power amplifiers. *IEEE Microw. Mag.* **2016**, *17*, 18–31. [CrossRef]
9. Freiberger, K.; Wolkerstorfer, M.; Enzinger, H.; Vogel, C. Digital predistorter identification based on constrained multi-objective optimization of WLAN standard performance metrics. In Proceedings of the 2015 IEEE International Symposium on Circuits and Systems (ISCAS), Lisbon, Portugal, 24–27 May 2015; pp. 862–865.
10. Li, L.; Ghazi, A.; Boutellier, J.; Anttila, L.; Valkama, M.; Bhattacharyya, S.S. Evolutionary multiobjective optimization for digital predistortion architectures. In Proceedings of the International Conference on Cognitive Radio Oriented Wireless Networks, Rome, Italy, 25–26 November 2016; pp. 498–510.
11. Mengozzi, M.; Gibiino, G.P.; Angelotti, A.M.; Florian, C.; Santarelli, A. Supply-modulated PA performance enhancement by joint optimization of RF input and supply control. In Proceedings of the IEEE Asia-Pacific Microwave Conference, Hong Kong, China, 8–11 December 2020; pp. 585–587.
12. Mengozzi, M.; Gibiino, G.P.; Angelotti, A.M.; Florian, C.; Santarelli, A. GaN power amplifier digital predistortion by multi-objective optimization for maximum RF output power. *Electronics* **2021**, *10*, 244. [CrossRef]
13. Mengozzi, M.; Angelotti, A.M.; Gibiino, G.P.; Florian, C.; Santarelli, A. Joint Dual-Input Digital Predistortion of Supply-Modulated RF PA by Surrogate-Based Multi-Objective Optimization. *IEEE Trans. Microw. Theory Tech.* **2021**, *70*, 35–49. [CrossRef]
14. Kantana, C.; Ma, R.; Benosman, M.; Komatsuzaki, Y. A Hybrid Heuristic Search Control Assisted Optimization of Dual-Input Doherty Power Amplifier. In Proceedings of the European Microwave Conference 2021, London, UK, 27–29 September 2022; pp. 126–129.
15. Wang, T.; Li, W.; Quaglia, R.; Gilabert, P.L. Machine-Learning Assisted Optimisation of Free-Parameters of a Dual-Input Power Amplifier for Wideband Applications. *Sensors* **2021**, *21*, 2831 . [CrossRef] [PubMed]
16. Campbell, C.F.; Tran, K.; Kao, M.Y.; Nayak, S. A K-band 5W Doherty amplifier MMIC utilizing 0.15 µm GaN on SiC HEMT technology. In Proceedings of the 2012 IEEE Compound Semiconductor Integrated Circuit Symposium (CSICS), La Jolla, CA, USA, 14–17 October 2012; pp. 1–4.

17. Valenta, V.; Davies, I.; Ayllon, N.; Seyfarth, S.; Angeletti, P. High-gain GaN Doherty power amplifier for Ka-band satellite communications. In Proceedings of the 2018 IEEE Topical Conference on RF/Microwave Power Amplifiers for Radio and Wireless Applications (PAWR), Anaheim, CA, USA, 14–17 January 2018; pp. 29–31.
18. Nakatani, K.; Yamaguchi, Y.; Komatsuzaki, Y.; Sakata, S.; Shinjo, S.; Yamanaka, K. A Ka-band high efficiency Doherty power amplifier MMIC using GaN-HEMT for 5G application. In Proceedings of the 2018 IEEE MTT-S International Microwave Workshop Series on 5G Hardware and System Technologies (IMWS-5G), Dublin, Ireland, 30–31 August 2018; pp. 1–3.
19. Shepphard, D.J.; Powell, J.; Cripps, S.C. An efficient broadband reconfigurable power amplifier using active load modulation. *IEEE Microw. Wirel. Compon. Lett.* **2016**, *26*, 443–445. [CrossRef]
20. Barmuta, P.; Gibiino, G.P.; Ferranti, F.; Lewandowski, A.; Schreurs, D.M.P. Design of experiments using centroidal Voronoi tessellation. *IEEE Trans. Microw. Theory Tech.* **2016**, *64*, 3965–3973. [CrossRef]
21. Miettinen, K. *Nonlinear Multiobjective Optimization*; Springer Science & Business Media: Berlin/Heidelberg, Germany, 2012; Volume 12.
22. Cidronali, A.; Giovannelli, N.; Vlasits, T.; Hernaman, R.; Manes, G. A 240W dual-band 870 and 2140 MHz envelope tracking GaN PA designed by a probability distribution conscious approach. In Proceedings of the IEEE MTT-S International Microwave Symposium Digest, Natal, Brazil, 5–10 June 2011; pp. 1–4.
23. Angelotti, A.M.; Gibiino, G.P.; Nielsen, T.S.; Santarelli, A.; Verspecht, J. Impact of Broadband Modulation in Active Load-Pull On-Wafer Measurements of GaN HEMTs. In Proceedings of the ARFTG Microwave Measurement Conference, Denver, CO, USA, 24 June 2022; pp. 1–4.
24. Rolain, Y.; Zyari, M.; Van Nechel, E.; Vandersteen, G. A measurement-based error-vector-magnitude model to assess non linearity at the system level. In Proceedings of the 2017 IEEE MTT-S International Microwave Symposium (IMS), Honolulu, HI, USA, 4–9 June 2017; pp. 1429–1432.
25. Gibiino, G.P.; Santarelli, A.; Schreurs, D.; Filicori, F. Two-input nonlinear dynamic model inversion for the linearization of envelope-tracking RF PAs. *IEEE Microw. Wirel. Compon. Lett.* **2016**, *27*, 79–81. [CrossRef]
26. Chani-Cahuana, J.; Landin, P.N.; Fager, C.; Eriksson, T. Iterative Learning Control for RF power amplifier linearization. *IEEE Trans. Microw. Theory Tech.* **2016**, *64*, 2778–2789. [CrossRef]
27. Frazier, P.I. A Tutorial on Bayesian Optimization. *arXiv* **2018**, arXiv:1807.02811.
28. Rasmussen, C.E.; Williams, C.K.I. *Gaussian Processes for Machine Learning*; Adaptive Computation and Machine Learning; MIT Press: Cambridge, MA, USA, 2006; pp. 1–248.
29. Snoek, J.; Larochelle, H.; Adams, R.P. Practical Bayesian Optimization of Machine Learning Algorithms. *arXiv* **2012**, arXiv:1206.2944v2.
30. Lafleur, J.M. Heuristic Method for Identifying Concave Pareto Frontiers in Multi-Objective Dynamic Programming Problems. *AIAA J.* **2014**, *52*, 496–503. [CrossRef]
31. Angelotti, A.M.; Gibiino, G.P.; Florian, C.; Santarelli, A. Broadband error vector magnitude characterization of a GaN power amplifier using a vector network analyzer. In Proceedings of the IEEE/MTT-S International Microwave Symposium Digest, Los Angeles, CA, USA, 4–6 June 2020; pp. 747–750.